Journal of Physics: Condensed Matter

PAPER

Quantum-confinement effect on the linewidth broadening of metal halide perovskite-based quantum dots

To cite this article: Hyun Myung Jang *et al* 2021 *J. Phys.: Condens. Matter* **33** 355702

View the article online for updates and enhancements.

You may also like

- Physics of biofilms: the initial stages of biofilm formation and dynamics
Guillaume Lambert, Andrew Bergman, Qiucen Zhang et al.
- Enhancing the Phase Stability of Formamidinium Lead Triiodide by Addition of Calcium Chloride
Jin Hyuck Heo, Nang Mya Su Aung, Seok Yeong Hong et al.
- OSNR and dispersion tolerance of FWM based optical carrier recovery scheme
Sachinthani Alahakoon, Dushani Munasinghe, Gresha S Samarakkody et al.

IOP ebooks™

Bringing together innovative digital publishing with leading authors from the global scientific community.

Start exploring the collection–download the first chapter of every title for free.

This content was downloaded from IP address 147.46.230.251 on 25/10/2021 at 11:51

IOP Publishing Journal of Physics: Condensed Matter
J. Phys.: Condens. Matter **33** (2021) 355702 (10pp) https://doi.org/10.1088/1361-648X/ac00db

Quantum-confinement effect on the linewidth broadening of metal halide perovskite-based quantum dots

Hyun Myung Jang[1,2,*], **Jinwoo Park**[2], **Sungjin Kim**[2] and **Tae-Woo Lee**[1,2,3,*]

[1] Research Institute of Advanced Materials (RIAM), Seoul National University, 1 Gwanak-ro, Gwanak-gu, Seoul 08826, Republic of Korea
[2] Department of Materials Science and Engineering, Seoul National University, 1 Gwanak-ro, Gwanak-gu, Seoul 08826, Republic of Korea
[3] School of Chemical and Biological Engineering, Institute of Engineering Research, Nano Systems Institute (NSI), Seoul National University, Seoul 08826, Republic of Korea

E-mail: jang0227@snu.ac.kr and twlees@snu.ac.kr

Received 19 March 2021, revised 21 April 2021
Accepted for publication 13 May 2021
Published 6 July 2021

Abstract

The linewidth broadening caused by various physicochemical effects does limit the well-known advantage of ultrahigh color purity of metal halide perovskites (MHPs) for use in next-generation light-emitting diodes (LEDs). We have theoretically examined the quantum- and dielectric-confinement effects of a quantum dot (QD) on the degree of photoluminescence linewidth broadening. It is predicted that the linewidth ($\Delta\lambda_{QC}$) is mainly contributed by the two opposing effects: (i) the linewidth broadening due to the repulsive kinetic energy of confined excitons ($\Delta\lambda_{QC}^{(KE)}$) and (ii) the overall linewidth narrowing caused by the attractive Coulomb interaction ($\Delta\lambda_{QC}^{(Coul)}$). It is shown that the relative contribution essentially remains at a constant value and is evaluated as $\Delta\lambda_{QC}^{(Coul)}/\Delta\lambda_{QC}^{(KE)} = 0.42$, which is independent of the QD size and the chemical nature of semiconducting emitter. We have computed $\Delta\lambda_{QC}$ for various QD sizes of the prototypical MHP emitter, $MAPbBr_3$, where MA denotes a methylammonium (CH_3NH_3) organic cation. The calculated results show that the linewidth broadening due to the quantum confinement ($\Delta\lambda_{QC}$) increases rapidly beginning at the QD radius approximately equal to 6.5 nm but $\Delta\lambda_{QC}$ is less than 2 nm even at $R = 1.5$ nm. Thus, $\Delta\lambda_{QC}$ is much narrower than the linewidth caused by the exciton-LO phonon Fröhlich coupling ($\sim$23.4 nm) which is known as the predominant mechanism of linewidth broadening in hybrid MHPs. Thus, the linewidth broadening due to the quantum confinement ($\Delta\lambda_{QC}$) is not a risk factor in the realization of MHP-based ultrahigh-quality next-generation LEDs.

Keywords: linewidth broadening, quantum confinement, exciton, metal halide perovskites, photoluminescence, light-emitting diodes

(Some figures may appear in colour only in the online journal)

1. Introduction

Metal halide perovskites (MHPs) show superior electrical and optical properties, which give them great potential for use in next-generation light-emitting diodes (LEDs) [1–4]. In particular, their narrow emission linewidths, as quantified by full width at half maximum (FWHM), can achieve ultra-high color purity: FWHM $\leqslant$ 20 nm and color gamut $\geqslant$ 140% in NTSC standard. These are superior to the properties of organic emitters (FWHM $>$ 40 nm and color gamut $<$ 100%

* Authors to whom any correspondence should be addressed.

 © 2021 IOP Publishing Ltd Printed in the UK

in NTSC standard) and inorganic quantum dot emitters (FWHM $\approx$ 30–40 nm and color gamut $\approx$ 120% in NTSC standard) [5]. However, the linewidth broadening caused by various physico-chemical effects potentially limits the well-known advantage of narrow emission linewidths (FWHM $\leqslant$ 20 nm) and, thus, ultrahigh color purity of MHPs [5, 6].

Several intrinsic and extrinsic factors are known to significantly influence the linewidth broadening of photoluminescent materials. For most semiconductors, these broadening factors (in FWHM) are decomposed into the following four main terms [7, 8]: $\Delta\lambda(T) = \Gamma_o + \Gamma_{\rm ac}(T) + \Gamma_{\rm LO}(T) + \Gamma_{\rm imp}$, where Γ_o denotes temperature-independent inhomogeneous line broadening that results from scattering due to disorder and imperfections. On the other hand, $\Gamma_{\rm ac}(T)(=\gamma_{\rm ac}T)$ and $\Gamma_{\rm LO}(T)(=\gamma_{\rm LO}N_{\rm LO}(T))$ are homogeneous broadening terms, which arise from acoustic and longitudinal optical (LO) phonon scatterings with the charge-carrier-phonon coupling strengths of $\gamma_{\rm ac}$ and $\gamma_{\rm LO}$, respectively. Here, $N_{\rm LO}(T)$ denotes the Bose–Einstein distribution function with $N_{\rm LO}(T) = 1/\left\{e^{\hbar\omega_{\rm LO}/k_{\rm B}T} - 1\right\}$, where $\hbar\omega_{\rm LO}$ is the characteristic energy of LO phonons. $\Gamma_{\rm imp}$ phenomenologically accounts for inhomogeneous scattering from ionized impurities.

In 2016, Wright and co-workers reported their systematic investigations on the linewidth broadening of several hybrid MHPs [9]: $MAPbBr_3$, $MAPbI_3$, $FAPbBr_3$, and $FAPbI_3$, where MA and FA, respectively, denote methylammonium (CH_3NH_3) and formamidinium ($CH(NH_2)_2$) organic cations. They have shown that the long-range Fröhlich coupling between exciton carriers and LO phonons is the major cause of linewidth broadening in hybrid MHPs at room temperature, where the scattering from acoustic phonons [$\Gamma_{\rm ac}(T)$] and impurities ($\Gamma_{\rm imp}$) is a minor component. Thus, the broadening factors can be simplified as $\Delta\lambda(T) = \Gamma_o + \Gamma_{\rm LO}(T)$. They obtained this conclusion by carefully monitoring the temperature-dependent FWHM of the photoluminescence (PL) peak and subsequently fitting it with the Bose–Einstein distribution function. In the case of $MAPbBr_3$ film, the FWHM of the room-temperature steady-state peak is 23.4 nm at λ = 538 nm (corresponding to $\Delta\omega_{\rm FWHM}$ = 100 meV), which slightly exceeds the high color-purity standard of FWHM $\leqslant$ 20 nm.

The PL efficiency itself is the most crucial factor in LEDs. It is now well known that the PL efficiency of perovskite emitters can be improved greatly if the exciton binding energy ($E_{\rm b}$) is increased and the exciton diffusion length ($L_{\rm D}$) is decreased by reducing the grain size [5, 6]. An ideal approach to achieve high $E_{\rm b}$ and low $L_{\rm D}$ in perovskite emitters is to effectively confine the excitons in the form of colloidal nanoparticles (NPs with the size $<$ 20 nm) rather than in polycrystalline perovskite bulk films having large grain sizes (0.1–10 μm) [6, 10]. NPs with their sizes less than the exciton Bohr diameter are called quasi-zero-dimensional quantum dots (quasi-0D QDs). They showed high $E_{\rm b}$ and low $L_{\rm D}$ and, thereby, achieved high photoluminescent quantum efficiency (PLQE) at room temperature [1, 11–15]. However, these quasi-0D QDs suffer from strong dependence of the emission wavelength (i.e., pronounced PL blue shift) and the linewidth broadening on the QD size, as do inorganic QDs [16].

In case of the PL blue shift with decreasing QD size, one can make use of this shift to the color tunability from green to blue. On the contrary, the linewidth broadening simply deteriorates the color purity. In this regard, it is of great importance to clearly elucidate the effect of the quantum-size confinement (or size reduction) on the degree of the PL linewidth broadening of perovskite emitters. In spite of its importance, little theoretical progress has been made in this subject. In consideration of this background, we have systematically examined and clarified the effect of the QD-size confinement on the degree of the PL linewidth broadening of $MAPbBr_3$, the prototypical MHP. However, our theoretical approach developed in the present study is not limited to hybrid MHP QDs but can be applied to various types of semiconducting QDs.

2. Linewidth broadening by quantum confinement

In this section, we will theoretically formulate the PL linewidth broadening due to the quantum-confinement effect which is independent of the linewidth broadening caused by the well-known carrier-LO phonon long-range Fröhlich coupling [9]. For this purpose, we will firstly examine the net energy of a confined exciton [$E_{\rm ext}(R;\alpha)$] in a given QD under the condition of simultaneous quantum and dielectric confinements. We will then theoretically formulate the uncertainty in the exciton's linear momentum [Δp] and its correlation with the uncertainty in the corresponding linewidth [$\Delta\lambda_{\rm QC}$] solely caused by the quantum confinement. As the third step, we will deduce the uncertainty product ($\Delta p\Delta x$) of an exciton confined in a QD by considering the ground-state exciton wave function [$\psi_o(x)$] and its Fourier transform [$g(k)$]. On the basis of all these formulations, we will finally obtain an expression of $\Delta\lambda_{\rm QC}$ in terms of the QD size (R), the PL wavelength (λ) and the effective Coulomb interaction coefficient.

2.1. Exciton energy under simultaneous quantum and dielectric confinements

If the relative dielectric permittivity of the surrounding medium or solvent is lower than that of the quantum dot (QD), the surrounding medium tends to exert a repulsive force on the central QD, raising a dielectric-confinement effect on the central QD. This situation actually corresponds to the measurement of high PLQE PL spectrum from the dispersed QDs in a surrounding low-permittivity medium [6, 10, 11]. Under this condition, the effective Coulomb interaction coefficient (C_1') is reduced from the well-known unmodified coefficient $C_1(=1.786)$ which corresponds to the purely quantum confinement in the absence of any dielectric-confinement effect for the (s–s)-type ground state of exciton [17–19]. In the below, we will theoretically correlate the modified interaction coefficient, C_1', with C_1 and the surface-polarization integral ($I_{\rm sp}$) which arises from the difference in the relative dielectric permittivity between the QD and the surrounding low-permittivity medium. We will subsequently show that the value

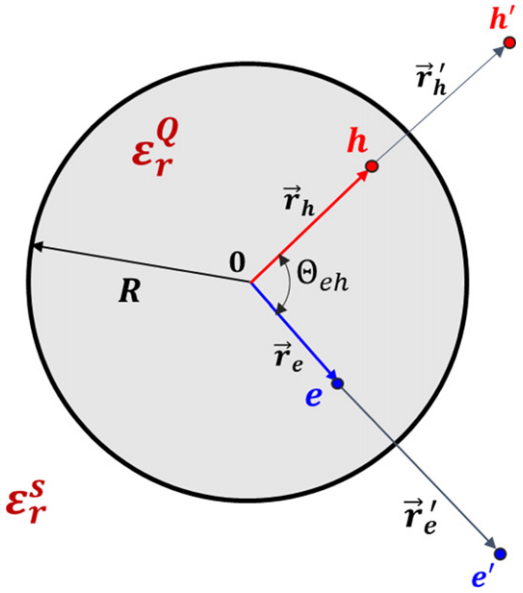

Figure 1. A schematic diagram of an exciton in a quasi-0D QD with the radius R. The spherical QD having the relative dielectric permittivity of ε_r^Q is immersed in a low-permittivity solvent medium of ε_r^s. The $\vec{r}_e$ and $\vec{r}_h$ vectors, respectively, denote the distances of the electron and the hole from the center of the QD. The image charges $e'(=\frac{\pm R\cdot e}{r_e})$ and $h'(=\frac{-R\cdot e}{r_h}=\frac{\pm R\cdot h}{r_h})$ are located at the distances $r_e'(=\frac{R^2}{r_e})$ and $r_h'(=\frac{R^2}{r_h})$, respectively, from the center of the QD.

of C_1' can be obtained numerically as a function of the permittivity ratio, $\varepsilon_r^Q/\varepsilon_r^s$, where ε_r^Q and ε_r^s, respectively, denote the dielectric constants (permittivities) of the central QD and the surrounding medium (figure 1).

To correlate the modified Coulomb interaction coefficient (C_1') with $C_1, \varepsilon_r^Q, \varepsilon_r^s$ and $I_{\rm sp}$, let us consider the Hamiltonian operator ($H_{\rm QD}$) of the confined exciton within the central spherical QD having the radius R. For this purpose, we use the following Brus–Takagahara-type standard form of H in the presence of the dielectric-confinement effect [20, 21]:

$$\begin{aligned} H_{\rm QD} = &-\frac{\hbar^2}{2m_e}\nabla_e^2 - \frac{\hbar^2}{2m_h}\nabla_h^2 - \frac{e^2}{4\pi\varepsilon_o\varepsilon_r^Q\,|r_e - r_h|} \\ &+ \frac{e^2}{4\pi\varepsilon_o\,(2R)}\sum_{n=0}^{\infty}(\bar{\varepsilon}_n)^{-1}\left\{\left(\frac{r_e}{R}\right)^{2n} + \left(\frac{r_h}{R}\right)^{2n}\right\} \\ &- \frac{e^2}{4\pi\varepsilon_o\,(R)}\sum_{n=0}^{\infty}(\bar{\varepsilon}_n)^{-1}\left(\frac{r_e r_h}{R^2}\right)^{n} P_n(\cos\,\Theta_{eh}) \\ &+ V(r_e, r_h), \end{aligned} \tag{1}$$

where r_e and r_h denote the coordinates of an electron and a hole, respectively, m_e and m_h are their effective masses, P_n is the Legendre polynomial of the nth order, and Θ_{eh} designates the angle between r_e and r_h. The potential energy, $V(r_e, r_h)$ describes the motion of the exciton quasi-particle within the QD simulated by an infinitely deep potential well. Thus, $V(r_e, r_h) = 0$ for $r_e, r_h \leqslant R$ and $V(r_e, r_h) = \infty$ for $r_e, r_h > R$. In equation (1), the dielectric-stiffness parameter, $(\bar{\varepsilon}_n)^{-1}$, is defined by

$$(\bar{\varepsilon}_n)^{-1} = \frac{(n+1)(\varepsilon - 1)}{\varepsilon_r^Q\,(n\varepsilon + n + 1)}, \tag{2}$$

where $\varepsilon = \varepsilon_r^Q/\varepsilon_r^s$. The first two terms in equation (1) represent the kinetic energy and the third term depicts the direct Coulomb interaction between an electron and a hole. The two terms that follow the third term correspond to the surface polarization energy which arises from the difference in the relative dielectric permittivity (ε_r) between the semiconducting QD and the surrounding solvent medium. The former (i.e., 4th term) represents the repulsive self-energy of an electron and a hole due to its own image charge ($V_{ee'}$ and $V_{hh'}$; figure 1), whereas the latter (i.e., 5th term) depicts the attractive interaction energy between an electron and a hole via image (wrong) charges ($V_{eh'}$ and $V_{he'}$).

The expectation value integral of the first three terms of the Hamiltonian operator ($\equiv H_{1-3}$), as calculated using the ground-state (s–s)-type wave function of exciton, leads to the following expression [17]:

$$\begin{aligned} \langle\psi_o^s(r_e, r_h; \alpha)\,|H_{1-3}|\,\psi_o^s(r_e, r_h; \alpha)\rangle = &\frac{\hbar^2\pi^2}{2\mu_o R^2} + \frac{\hbar^2}{2\mu_o}\left(\frac{1}{\alpha}\right)^2 \\ &- \frac{C_1 e^2}{4\pi\varepsilon_o\varepsilon_{r(R)}^Q R} \\ &- \frac{C_2 e^2}{4\pi\varepsilon_o\varepsilon_{r(R)}^Q \alpha}, \end{aligned} \tag{3}$$

where μ_o is the effective reduced mass of exciton (i.e., $\frac{1}{\mu_o} \equiv \frac{1}{m_e^*} + \frac{1}{m_h^*}$) and $C_2 = 0.498$. On the other hand, C_1 denotes the unmodified Coulomb interaction coefficient $[= 2 - \pi^{-1}\left\{Si(2\pi) - 2^{-1}Si(4\pi)\right\} = 1.786]$ which corresponds to the purely quantum confinement in the absence of any dielectric-confinement effect [17, 18]. Equation (3) is the most elaborate expression of the net exciton energy above the bulk band gap, which considers the internal relative motion between the electron and hole in a given exciton [17]. This internal correlation effect can be implemented by including the e–h correlation parameter (α) in the ground-state wave function $\psi_o^s(r_e, r_h; \alpha)$, where $\psi_o^s(r_e, r_h; \alpha)$ is given by [17].

$$\begin{aligned} \psi_o^s(r_e, r_h; \alpha) &= C j_o\left(\frac{\pi r_e}{R}\right) j_o\left(\frac{\pi r_h}{R}\right)\exp\left(-\frac{r_{eh}}{\alpha}\right) \\ &= C\frac{\sin\left(\frac{\pi r_e}{R}\right)}{r_e}\frac{\sin\left(\frac{\pi r_h}{R}\right)}{r_h}\exp\left(-\frac{r_{eh}}{\alpha}\right), \end{aligned} \tag{4}$$

where j_o is the zeroth degree spherical Bessel function and r_{eh} denotes the distance between the electron and hole in a given exciton quasi-particle. The normalization constant (C) can be evaluated by imposing the following normalization condition [17]: $\int_0^R dr_e \int_0^R dr_h \int_{|r_e - r_h|}^{|r_e + r_h|} dr_{eh}\, r_e r_h r_{eh} |\psi_o^s(r_e, r_h; \alpha)|^2 = 1$. Detailed mathematical treatments on the evaluation of C are given in appendix of reference [21]. As shown in equation (4), the parameter α, appears in the correlation part, $\left[\exp(-r_{eh}/\alpha)\right]$, of the ground-state wave function for a spherical QD [17] or a cubic QD [22]. According to equation (3), the expectation value of the attractive Coulomb interaction energy within a QD (in the absence of any dielectric-confinement

effect) is, thus, given by the following expression [17]:

$$\langle E_{\mathrm{Coul}}\rangle = -\frac{C_1 e^2}{4\pi\varepsilon_o\varepsilon^{Q}_{r(R)}R} - \frac{C_2 e^2}{4\pi\varepsilon_o\varepsilon^{Q}_{r(R)}\alpha} < 0. \tag{5}$$

Let us now consider the remaining two terms of the Hamiltonian that corresponds to the surface polarization energy (E_{SP}). The 4th term of equation (1) corresponds to the repulsive self-interaction ($H_{\mathrm{SI}} = V_{ee'} + V_{hh'}$) of the hole and electron with their own images. On the contrary, the 5th term depicts the energies of interaction of the hole and electron with the 'wrong' images ($H_{\mathrm{WI}} = V_{eh'} + V_{he'}$). Takagahara evaluated this self-polarization term to assess the dielectric-confinement effect [21]. According to our notation, the expectation value of this self-polarization term can be written as

$$\begin{aligned}\langle E_{\mathrm{SP}}\rangle &= \langle\psi^s_o(r_e, r_h;\alpha)\,|H_{\mathrm{SP}}|\psi^s_o(r_e, r_h;\alpha)\rangle \\ &= \frac{\left\{2\pi^{-2}I_{\mathrm{sp}} - (\bar{\varepsilon}_0)^{-1}\right\}e^2}{4\pi\varepsilon_o\varepsilon^{Q}_{r(\infty)}R} \equiv \frac{+\Delta C e^2}{4\pi\varepsilon_o\varepsilon^{Q}_{r(R)}R},\end{aligned} \tag{6}$$

where $H_{\mathrm{SP}} = H_{\mathrm{SI}} + H_{\mathrm{WI}}$, $(\bar{\varepsilon}_0)^{-1} = \frac{1}{\varepsilon^s_r} - \frac{1}{\varepsilon^{Q}_r}$ according to equation (2), and the integral I_{sp} (equal to I_3 in Takagahara's notation [21]) is defined as

$$I_{\mathrm{sp}} = \pi\int_0^{\pi} \mathrm{d}x\,\sin^2 x \sum_{n=0}^{\infty}(\bar{\varepsilon}_n)^{-1}\left(\frac{x}{\pi}\right)^{2n}. \tag{7}$$

It should be noted that $\varepsilon^{Q}_{r(\infty)}$ appeared in the 3rd term of equation (6) is the relative dielectric permittivity of the QD constituting material in the bulk unconfined state where $R\to\infty$ and, thus, it is not equal to $\varepsilon^{Q}_{r(R)}$ appeared in the 4th term. Here, we are mainly interested in the effect of dielectric confinement on the modified interaction coefficient (C_1') in the vicinity of the critical size (R_{c}) that corresponds to the onset of the PL blue shift. Since the band gap at R_{c} is equal to the bulk band gap, $E_{\mathrm{g(b)}}$, $\varepsilon^{Q}_{r(R)}$ at R_{c} can be safely replaced by $\varepsilon^{Q}_{r(\infty)}$. Under this condition, the last expression of equation (6) is permissible. Thus, the effective Coulomb interaction coefficient (C_1') modified by the dielectric-confinement effect is given by

$$C_1' \equiv C_1 - \Delta C = C_1 - \left\{2\pi^{-2}I_{\mathrm{sp}} - (\bar{\varepsilon}_0)^{-1}\right\} = -\frac{1}{2}A_1. \tag{8}$$

As shown in equation (8), there is a distinct difference between the two contributions, C_1 and ΔC, to the modified interaction coefficient. The unmodified Coulomb interaction coefficient $C_1(=1.786)$ is related exclusively to the pure quantum-confinement effect in the absence of any low-permittivity dielectric medium. The presence of the surrounding low-permittivity dielectric medium provides an additional confinement effect on a QD [21]. This repulsive dielectric-confinement effect always leads to a decrease in the effective Coulomb-interaction coefficient by ΔC. The last expression of equation (8) is written to correlate C_1' with the notation of Takagahara [21]. Thus, $A_1 = -2C_1'$. Takagahara numerically evaluated A_1 as a function of the permittivity ratio, $\left(\varepsilon^{Q}_r/\varepsilon^s_r\right)$ [21]. Thus, one can evaluate C_1' for various values of $\left(\varepsilon^{Q}_r/\varepsilon^s_r\right)$ using equation (8). As reflected in equation (8), I_{sp} is a measure of the repulsive dielectric-confinement effect. On the contrary, $(\bar{\varepsilon}_0)^{-1}(>0)$ tends to increase the degree of attractive Coulomb interaction and gives a negative contribution to the dielectric-confinement effect. On the other hand, the unmodified Coulomb interaction coefficient (C_1), which corresponds to the pure quantum-confinement effect, is given by

$$C_1 = 1.786 = \frac{4I_{\mathrm{DC}}}{\pi} = \frac{4}{\pi}\int_0^{\pi}\mathrm{d}x_e\int_0^{\pi}\mathrm{d}x_h\frac{1}{x_>}\sin^2 x_e\sin^2 x_h, \tag{9}$$

where $x_> = \max(x_e, x_h)$. The integral I_{DC} is equal to I_2 in Takagahara's notation [21].

Combining equations (1), (3), and (6), one can obtain the following expression of the net exciton energy above the bulk band gap or the band-gap increment [$\delta E_{\mathrm{g}}(R;\alpha)$] with an arbitrary degree of the e–h correlation:

$$\begin{aligned}\delta E_{\mathrm{g}}(R;\alpha) &= \langle\psi^s_o(r_e, r_h;\alpha)\,|H_{\mathrm{QD}}|\psi^s_o(r_e, r_h;\alpha)\rangle \\ &= \frac{\hbar^2\pi^2}{2\mu_o R^2} - \frac{C_1' e^2}{4\pi\varepsilon_o\varepsilon^{Q}_{r(R)}R} \\ &\quad + \frac{\hbar^2}{2\mu_o}\left(\frac{1}{\alpha}\right)^2 - \frac{C_2 e^2}{4\pi\varepsilon_o\varepsilon^{Q}_{r(R)}\alpha}.\end{aligned} \tag{10}$$

Equation (10) is a starting point of further analysis of various exciton-related physical properties. Let us now consider the ratio of the two distinct proportionality terms appeared in equation (10).

$$\left(\frac{e^2}{4\pi\varepsilon_o\varepsilon^{Q}_{r(R)}}\right)\Big/\left(\frac{\hbar^2}{2\mu_o}\right) = \frac{2\mu_o e^2}{4\pi\varepsilon_o\varepsilon^{Q}_{r(R)}\hbar^2} \equiv \frac{2}{a_{B(R)}}, \tag{11}$$

where $a_{\mathrm{B}(R)}$ in equation (11) is the effective e–h radius for a confined exciton and, thus, it is different from the exciton Bohr radius for the bulk exciton $\left(a_{\mathrm{B}(\infty)}\right)$. The exciton Bohr radius for the bulk unconfined state is given by the well-known Griffiths equation, $a_{\mathrm{B}(\infty)} = \frac{4\pi\varepsilon_o\varepsilon^{Q}_{r(\infty)}\hbar^2}{\mu_o e^2}$, where $R\to\infty$ and $\varepsilon^{Q}_{r(\infty)}$ designates the relative dielectric permittivity of the QD-constituting bulk semiconductor with the absence of any confinement effect. Incorporating equation (11) into equation (10) then yields

$$\delta E_{\mathrm{g}}(R;\alpha) = \frac{\hbar^2}{2\mu_o}\left[\left\{\frac{\pi^2}{R^2} + \left(\frac{1}{\alpha}\right)^2\right\} - \frac{2}{a_{\mathrm{B}(R)}}\left\{\frac{C_1'}{R} + \frac{C_2}{\alpha}\right\}\right]. \tag{12}$$

2.2. Uncertainty in the linear momentum in terms of linewidth broadening

The band-gap increment associated with the PL blue shift $\left[\delta E_{\mathrm{g}}(R;\alpha)\right]$ can also be correlated with its PL frequency or wavelength by the Planck condition:

$$\delta E_{\mathrm{g}}(R;\alpha) \equiv \hbar\omega - E_{\mathrm{g(b)}} = \hbar\omega - \hbar\omega_o = \hbar\left\{\frac{2\pi c}{\lambda} - \frac{2\pi c}{\lambda_o}\right\}, \tag{13}$$

where $\hbar\omega_o$ denotes the energy corresponding to the bulk band gap $\left(E_{\mathrm{g(b)}}\right)$. Thus, $E_{\mathrm{g(b)}} = \hbar\omega_o = \frac{2\pi c\hbar}{\lambda_o}$. We can experimentally

find λ_o by measuring the PL wavelength at the onset of PL blue shift. On the contrary, λ is the characteristic PL wavelength of a confined QD having the radius R.

Combining equation (12) with equation (13), one can obtain the following relation for the uncertainty in the exciton energy $[\Delta\left(\delta E_{\mathrm{g}}\right)]$ in terms of five relevant uncertainties:

$$\begin{aligned}\Delta\left(\delta E_{\mathrm{g}}(R;\alpha)\right) &= \frac{\hbar^2}{2\mu_o}\left\{\pi^2\Delta\left(\frac{1}{R^2}\right) - \frac{2C_1'}{a_{\mathrm{B}(R)}}\Delta\left(\frac{1}{R}\right)\right.\\ &\quad\left. + \Delta\left(\frac{1}{\alpha^2}\right) - \frac{2C_2}{a_{\mathrm{B}(R)}}\Delta\left(\frac{1}{\alpha}\right)\right\}\\ &= \frac{2\pi c\hbar}{\lambda_o}\Delta\left\{\frac{(\lambda_o-\lambda)}{\lambda}\right\}. \end{aligned} \tag{14}$$

The four uncertainties in equation (14) can be expanded to yield the following forms:

$$\begin{aligned}\Delta\left(\frac{1}{R}\right) &= \left\{\frac{1}{\left(R-\frac{1}{2}\Delta R\right)} - \frac{1}{\left(R+\frac{1}{2}\Delta R\right)}\right\}\\ &= \frac{\Delta R}{\left\{R^2-\frac{1}{4}(\Delta R)^2\right\}} \approx \frac{\Delta R}{R^2}\end{aligned} \tag{15}$$

$$\begin{aligned}\Delta\left(\frac{1}{\alpha}\right) &= \left\{\frac{1}{\left(\alpha-\frac{1}{2}\Delta\alpha\right)} - \frac{1}{\left(\alpha+\frac{1}{2}\Delta\alpha\right)}\right\}\\ &= \frac{\Delta\alpha}{\left\{\alpha^2-\frac{1}{4}(\Delta\alpha)^2\right\}} \approx \frac{\Delta\alpha}{\alpha^2}\end{aligned} \tag{16}$$

$$\begin{aligned}\Delta\left(\frac{1}{R^2}\right) &= \left\{\frac{1}{\left(R-\frac{1}{2}\Delta R\right)^2} - \frac{1}{\left(R+\frac{1}{2}\Delta R\right)^2}\right\}\\ &= \frac{2R\Delta R}{\left\{R^2-\frac{1}{4}(\Delta R)^2\right\}^2} \approx \frac{2\Delta R}{R^3}\end{aligned} \tag{17}$$

$$\begin{aligned}\Delta\left(\frac{1}{\alpha^2}\right) &= \left\{\frac{1}{\left(\alpha-\frac{1}{2}\Delta\alpha\right)^2} - \frac{1}{\left(\alpha+\frac{1}{2}\Delta\alpha\right)^2}\right\}\\ &= \frac{2\alpha\Delta\alpha}{\left\{\alpha^2-\frac{1}{4}(\Delta\alpha)^2\right\}^2} \approx \frac{2\Delta\alpha}{\alpha^3}.\end{aligned} \tag{18}$$

Here, $\Delta R/2$ can be viewed as the uncertainty in R and $\Delta\alpha/2$ as the uncertainty in α. We will later show that ΔR for fixed R and λ is proportional to the uncertainty in the linear momentum of exciton. On the other hand, the uncertainty in the wavelength ratio in equation (14) can be expanded to yield the following form:

$$\begin{aligned}\Delta\left\{\frac{(\lambda_o-\lambda)}{\lambda}\right\} &= \left\{\frac{\lambda_o}{\left(\lambda-\frac{1}{2}\Delta\lambda_{\mathrm{QC}}\right)} - 1\right\}\\ &\quad - \left\{\frac{\lambda_o}{\left(\lambda+\frac{1}{2}\Delta\lambda_{\mathrm{QC}}\right)} - 1\right\}\\ &= \frac{\lambda_o\Delta\lambda_{\mathrm{QC}}}{\left\{\lambda^2-\frac{1}{4}\left(\Delta\lambda_{\mathrm{QC}}\right)^2\right\}} \approx \frac{\lambda_o\Delta\lambda_{\mathrm{QC}}}{\lambda^2}.\end{aligned} \tag{19}$$

Here, $\frac{1}{2}\Delta\lambda_{\mathrm{QC}}$ can be viewed as the uncertainty in λ and $\Delta\lambda_{\mathrm{QC}}$ thus denotes the FWHM of a hypothetical PL spectrum which would be solely caused by the quantum and dielectric confinements.

Substituting equations (15) and (19) into equation (14) yields

$$\begin{aligned}\Delta\left(\delta E_{\mathrm{g}}(R;\alpha)\right) &= \frac{\hbar^2}{\mu_o}\left\{\frac{\pi^2\Delta R}{R^3} + \frac{\Delta\alpha}{\alpha^3}\right\}\\ &\quad - \frac{\hbar^2}{\mu_o a_{\mathrm{B}(R)}}\left\{\frac{C_1'\Delta R}{R^2} + \frac{C_2\Delta\alpha}{\alpha^2}\right\} = \frac{hc\Delta\lambda_{\mathrm{QC}}}{\lambda^2}.\end{aligned} \tag{20}$$

The 1st term in the 2nd expression of equation (20) represents the uncertainty in the kinetic energy, $\Delta(E_k)$. This is because we have the following equality:

$$\Delta(E_k) = \frac{\hbar^2\pi^2}{2\mu_o}\Delta\left(\frac{1}{R^2}\right) = \frac{\hbar^2\pi^2\Delta R}{\mu_o R^3} = \frac{h^2\Delta R}{4\mu_o R^3}, \tag{21}$$

where h denotes the Planck constant ($=2\pi\hbar$). On the other hand, we can establish the following relation if we treat an exciton as a translationally moving point particle (at its center-of-mass) with the linear momentum, p:

$$\begin{aligned}\Delta(E_k) &= \frac{\Delta\left(p^2\right)}{2\mu_o} = \frac{1}{2\mu_o}\left\{\left(\overline{p}+\frac{1}{2}\Delta p\right)^2 - \left(\overline{p}-\frac{1}{2}\Delta p\right)^2\right\}\\ &= \frac{\overline{p}\Delta p}{\mu_o} = \frac{h\Delta p}{\mu_o\lambda}.\end{aligned} \tag{22}$$

In obtaining the last expression of equation (22), we used the following well-known De Broglie relation: $\overline{p} = \hbar\overline{k} = \frac{h}{2\pi}\frac{2\pi}{\lambda}$. Combining equation (21) with equation (22), we obtain the following relation between ΔR and Δp:

$$\frac{1}{2}\Delta\left(\frac{1}{R^2}\right) = \frac{\Delta R}{R^3} = \frac{4\Delta p}{h\lambda}. \tag{23}$$

Thus, the uncertainty in the QD size is directly corelated with the uncertainty in the linear momentum of exciton. Substituting equation (23) into equation (20) for ΔR leads to the following equation:

$$\begin{aligned}\Delta\left(\delta E_{\mathrm{g}}\right) &= \frac{\hbar^2}{\mu_o}\left\{\frac{\pi^2}{R} - \frac{C_1'}{a_{\mathrm{B}(R)}}\right\}\frac{\Delta R}{R^2}\\ &\quad + \frac{\hbar^2}{\mu_o}\left(\frac{\Delta\alpha}{\alpha^2}\right)\left\{\frac{1}{\alpha} - \frac{C_2}{a_{\mathrm{B}(R)}}\right\}\\ &= \frac{\hbar^2}{\mu_o R}\left\{\pi^2 - \frac{C_1'R}{a_{\mathrm{B}(R)}}\right\}\frac{4R\Delta p}{h\lambda}\\ &\quad + \frac{\hbar^2}{\mu_o}\left(\frac{\Delta\alpha}{\alpha^2}\right)\left\{\frac{1}{\alpha} - \frac{C_2}{a_{\mathrm{B}(R)}}\right\} = \frac{hc\Delta\lambda_{\mathrm{QC}}}{\lambda^2}.\end{aligned} \tag{24}$$

Thus, we are able to correlate the linewidth broadening ($\Delta\lambda_{\mathrm{QC}}$) with the uncertainty in the linear momentum of a confined exciton (Δp) and with the uncertainty in the quantum e–h correlation parameter ($\Delta\alpha$).

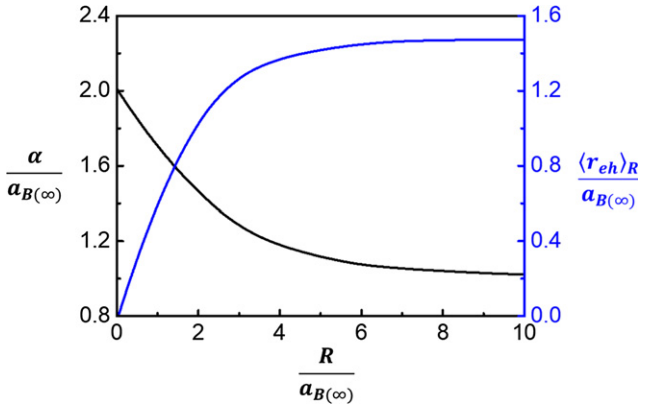

Figure 2. Quantum variationally optimized α *vs* $\cdot R$ and $\langle r_{eh}\rangle_R$ *vs* $\cdot R$ curves as obtained by Kayanuma [17]. Herein, $\langle r_{eh}\rangle_R$ denotes the mean distance between an electron and a hole in a given exciton pair which is confined in a quasi-0D QD with the radius R. Adapted with permission from Kayanuma (1986 *Solid State Commun.* **59** 405). Copyright 1986 Pergamon Press (Elsevier Ltd).

According to the quantum variational optimization (i.e., minimization) by Kayanuma [17], the following simple approximate relation can be written for $R \geqslant \sim 6a_{\mathrm{B}(\infty)}$:

$$\langle r_{eh}\rangle_{\infty} \approx \frac{3}{2} a_{\mathrm{B}(\infty)}, \tag{25}$$

where $\langle r_{eh}\rangle_{\infty}$ and $a_{\mathrm{B}(\infty)}$, respectively, denote the mean distance between an electron and a hole in a given exciton pair and the exciton Bohr radius in the bulk unconfined state. On the contrary, the mean electron–hole distance, $\langle r_{eh}\rangle_R$, is not constant but tends to decrease with decreasing QD radius [17]. From the result of quantum variational simulation [17], we have extracted the following simple relation between $\langle r_{eh}\rangle_R$ and the QD radius for $0 < R < 2a_{\mathrm{B}(\infty)}$ (figure 2):

$$\frac{\langle r_{eh}\rangle_R}{a_{\mathrm{B}(\infty)}} = \frac{1}{2}\left(\frac{R}{a_{\mathrm{B}(\infty)}}\right). \tag{26}$$

Considering a simple proportionality relation given in equation (25), one can write the following simple rule: $\langle r_{eh}\rangle_R / \langle r_{eh}\rangle_{\infty} \approx a_{\mathrm{B}(R)}/a_{\mathrm{B}(\infty)}$, where $a_{\mathrm{B}(R)}$ denotes the variable exciton Bohr radius for a confined exciton in a QD having the radius R. Then, combining this ratio with equation (25) yields

$$\langle r_{eh}\rangle_R = \frac{S}{2} a_{\mathrm{B}(R)}. \tag{27}$$

Considering the structure of equation (25), one can reason that the proportionality constant S is very close to 3. Using the definition of the Griffiths equation, one can readily show that $S = 3$ corresponds to the following relation: $\langle r_{eh}\rangle_R = \left\{\varepsilon_r^Q(R)/\varepsilon_r^Q(\infty)\right\}\langle r_{eh}\rangle_{\infty}$. This indicates that $\varepsilon_r^Q(R) < \varepsilon_r^Q(\infty)$ because $\langle r_{eh}\rangle_R < \langle r_{eh}\rangle_{\infty}$. In addition to this, $\langle r_{eh}\rangle_R$ decreases with decreasing QD size (figure 2) and asymptotically approaches $\langle r_{eh}\rangle_{\infty}/\varepsilon_r^Q(\infty)$ because $\varepsilon_r^Q\,(R \to a_o) = 1$, where a_o is the atomic Bohr radius $\left(\equiv \frac{4\pi\varepsilon_o\hbar^2}{m_e e^2} = 0.0529\ \mathrm{nm}\right)$. Substituting equation (27) into equation (26) then yields a simple linear relation between $a_{\mathrm{B}(R)}$ and the QD radius for $a_o < R < 2a_{\mathrm{B}(\infty)}$:

$$a_{\mathrm{B}(R)} = \frac{1}{S}R \approx \frac{1}{3}R. \tag{28}$$

Thus, the asymptotic lower limit of $a_{\mathrm{B}(R)}$ is $\frac{a_o}{3}$. On the other hand, the bulk exciton Bohr radius ($a_{\mathrm{B}(\infty)}$) can be numerically estimated using the Griffiths equation if μ_o and $\varepsilon_{r(\infty)}^Q$ are known. In the case of $MAPbBr_3$, $\mu_o = 0.117m_o$ [23] and $\varepsilon_{r(\infty)}^Q \approx 11$ were adopted from the Griffiths equation and the onset of the strong PL peak shift with decreasing R at room temperature [24]. Taking these two values, we deduce the following result: $a_{\mathrm{B}(\infty)} = \frac{4\pi\varepsilon_o\varepsilon_{r(\infty)}^Q\hbar^2}{\mu_o e^2} = \frac{1.11\times10^{-10}\times11\times\left(1.054\times10^{-34}\right)^2}{0.117\times9.11\times10^{-31}\times\left(1.602\times10^{-19}\right)^2} \approx 5.0$ (nm) [24]. Thus, one can expect that equation (28) is valid for the QD radius up to ~10 nm. Substituting equation (28) into equation (24) yields the following expression of the uncertainty in the band-gap increment:

$$\begin{aligned}\Delta\left(\delta E_{\mathrm{g}}\right) &= \frac{\hbar^2}{\mu_o R}\left\{\pi^2 - 3C_1'\right\}\frac{4R\Delta p}{h\lambda} \\ &\quad + \frac{\hbar^2}{\mu_o}\left(\frac{\Delta\alpha}{\alpha^2}\right)\left\{\frac{1}{\alpha} - \frac{3C_2}{R}\right\} \\ &= \frac{hc\Delta\lambda_{\mathrm{QC}}}{\lambda^2}.\end{aligned} \tag{29}$$

One should replace $\left(\frac{\Delta\alpha}{\alpha^2}\right)$-terms by Δp-containing terms to correlate the uncertainty in the exciton's momentum with the corresponding PL linewidth broadening.

Let us then express the quantum correlation parameter (α) in terms of the QD radius to suitably replace $\left(\frac{\Delta\alpha}{\alpha^2}\right)$-terms by Δp-containing terms. Using the result of quantum variational optimization [17], we have extracted the following simple linear relation between the e–h correlation parameter (α) and the QD radius for $R < \sim 2.3a_{\mathrm{B}(\infty)}$ (figure 2):

$$\alpha = -sR + 2.0a_{\mathrm{B}(\infty)}, \tag{30}$$

where the slope ($-s$) of $\Delta\alpha/\Delta R$ has an optimum numerical value of -0.27 [17].

Thus, we have: $\Delta(\alpha) = -s\Delta R$. Using these two expressions, we obtain

$$\left(\frac{\Delta\alpha}{\alpha^2}\right) = \frac{-s\Delta R}{\left(-sR + 2.0a_{\mathrm{B}(\infty)}\right)^2} = \frac{-4sR^3\Delta p}{h\lambda\left(-sR + 2.0a_{\mathrm{B}(\infty)}\right)^2}. \tag{31}$$

In obtaining the last expression, we used the $\Delta R - \Delta p$ relation presented in equation (23). Substituting equation (31) into equation (29) and rearranging the resulting relation, we eventually obtain the following equation that relates the uncertainty in the linear momentum (Δp) to the linewidth broadening due to the quantum-confinement effect $\left(\Delta\lambda_{\mathrm{QC}}\right)$:

$$\Delta p = \frac{\mu_o c\pi^2\Delta\lambda_{\mathrm{QC}}}{R\lambda\left\{\left(\pi^2 - 3C_1'\right)\frac{1}{R} + \frac{sR^2\left(\frac{3C_2}{R} - \frac{1}{\alpha}\right)}{\left(-sR + 2.0a_{\mathrm{B}(\infty)}\right)^2}\right\}}. \tag{32}$$

In section 2.3, we will exploit equation (32) to predict $\Delta\lambda_{\mathrm{QC}}$ in terms of R and λ by combining it with the uncertainty product of the ground-state exciton confined in a QD.

2.3. The uncertainty product and linewidth broadening

Considering the center-of-mass motion, one can regard the exciton as a neutral single particle moving inside a semiconducting QD having an infinite potential well. Thus, the QD potential $V(r) = 0$ for $0 \leqslant r \leqslant R$, where r is the position of exciton's center-of-mass from the center of QD. Let the wave function of the exciton confined in a QD has the following standard form because of the spherical symmetry: $\psi(r, \theta, \phi) = R_{nl}(r)\, Y_{lm}(\theta, \phi) = A R_{nl}(r)$, where $R_{nl}(r)$ denotes the radial wave function. Then, $R_{nl}(r)$ satisfies the following nonlinear Schrödinger equation:

$$\frac{\mathrm{d}^2 R_{nl}}{\mathrm{d}r^2} + \frac{2}{r}\frac{\mathrm{d}R_{nl}}{\mathrm{d}r} + \left(k^2 - \frac{l(l+1)}{r^2}\right) R_{nl} = 0, \qquad (33)$$

with $k^2 \equiv 2m_s E_k/\hbar^2$, where m_s can be identified as the sum of electron and hole effective masses, $k = \pi/R$, and $\hbar k$ as the sum of electron and hole momentums. The ground-state solution of the above 2nd-order nonlinear differential equation is given by the 0th order spherical Bessel function [$j_o(r) \sim \sin kr/kr$] for describing the motion of the exciton point-particle at its ground state (having $n = l = 0$) with the kinetic energy E_k. We then obtain the ground-state wave function of the exciton point-particle undergoing one-dimensional translational motion (ignoring the relative motion between the electron and hole) by replacing the notation for the radial coordinate (r) by x and $j_o(r)$ by $\psi_o(x)$:

$$\psi_o(x) = A\frac{\sin\left(R_o^{-1}x\right)}{x} = \sqrt{\frac{R_o}{\pi}}\frac{\sin\left(R_o^{-1}x\right)}{x} = \frac{\sqrt{R}}{\pi}\frac{\sin\left(\frac{\pi x}{R}\right)}{x}, \qquad (34)$$

where $R_o \equiv \frac{R}{\pi}$. The normalization constant 'A' appeared in equation (34) is evaluated by imposing the following equality: $1 = \int_{-\infty}^{+\infty} |\psi_o(x)|^2 \mathrm{d}x$. Since we are mainly concerned with the uncertainty in the translational momentum of the exciton point-particle, we deliberately ignore the e–h correlation part of the wave function, $\exp\left(-\frac{r_{eh}}{\alpha}\right)$, which describes the internal relative motion between the electron and hole in a given e–h pair.

Taking the Fourier transform of $\psi_o(x)$ into the momentum space, we obtain

$$\begin{aligned} g(k) &= \frac{1}{\sqrt{2\pi}}\int_{-\infty}^{+\infty} \psi_o(x)\, \mathrm{e}^{+\mathrm{i}kx}\, \mathrm{d}x \\ &= \sqrt{\frac{R_o}{\pi}} \cdot \frac{1}{\sqrt{2\pi}}\int_{-\infty}^{+\infty} \frac{\sin\left(R_o^{-1}x\right)}{x}\mathrm{e}^{+\mathrm{i}kx}\, \mathrm{d}x \\ &= \sqrt{\frac{R_o}{\pi}} \cdot \sqrt{\frac{\pi}{2}} = \sqrt{\frac{R}{2\pi}}. \end{aligned} \qquad (35)$$

In obtaining the right-hand-side of equation (35), we used the following result of Fourier transform:

$$\overline{g}(k) \equiv \frac{1}{\sqrt{2\pi}}\int_{-\infty}^{+\infty} \frac{\sin\left(R_o^{-1}x\right)}{x}\mathrm{e}^{+\mathrm{i}kx}\, \mathrm{d}x = \sqrt{\frac{\pi}{2}} \quad \text{if } k < \frac{\pi}{R}. \qquad (36)$$

Thus, equation (35) is valid for $k < \frac{\pi}{R} = \frac{1}{R_o}$. Therefore, the probability distribution of the exciton momentum ($\hbar k$) can be written as

$$|g(k)|^2 = \frac{R}{2\pi}. \qquad (37)$$

The FWHM of $|g(k)|^2$ is $\frac{2\pi}{R}$ (figure 3(a)), which can be deduced from the normalization: $1 = \int_{-\infty}^{+\infty} |g(k)|^2\, \mathrm{d}k$. Thus, the uncertainty in the exciton's wave number is $\frac{\pi}{R}\left(= \frac{1}{2}\ \text{FWHM}\right)$, namely

$$\Delta k = \frac{\pi}{R}. \qquad (38)$$

Let us then consider the square of the exciton wave function to deduce the uncertainty in the exciton's position:

$$|\psi_o(x)|^2 = \frac{R}{\pi^2}\frac{\sin^2\left(\frac{\pi x}{R}\right)}{x^2}. \qquad (39)$$

The uncertainty in the exciton's position can be deduced from the probability distribution, $|\psi_o(x)|^2$, which is plotted as a function of x from the center of QD (figure 3(b)). Thus, the uncertainty in the position $\left(= \frac{1}{2}\ \text{FWHM}\right)$ is

$$\Delta x \approx \frac{R}{2}. \qquad (40)$$

On the other hand, the uncertainty in the wave number is $\Delta k = \frac{\pi}{R}$ as given in equation (38). Thus, the uncertainty

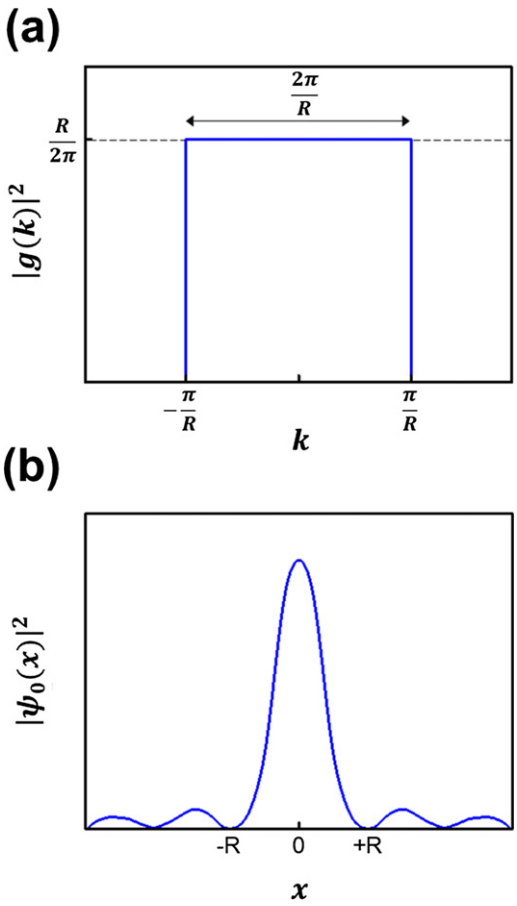

Figure 3. (a) The $|g(k)|^2$ *vs* $\cdot\, k$ plot, showing the probability distribution of the exciton momentum, $\hbar\boldsymbol{k}$. (b) The $|\psi_o(x)|^2$ *vs* $\cdot\, x$ plot, showing the probability distribution of the x-dependent exciton quasi-particle.

product of the exciton, which is confined in a QD having the radius R, is given by the following relation:

$$\Delta p\Delta x = \hbar\Delta k\Delta x = \hbar\frac{\pi}{R}\frac{R}{2} = \frac{\pi}{2}\hbar \approx \frac{3}{2}\hbar. \tag{41}$$

Thus, we can remove the inequality relation in the uncertainty product (i.e., $\Delta p\Delta x \geqslant \frac{\hbar}{2}$) and express the uncertainty product explicitly using the above equality relation. We will use equation (41) in predicting the contribution of the quantum confinement of exciton $\left(\Delta\lambda_{\mathrm{QC}}\right)$ to the net linewidth broadening in the PL spectrum.

Combining equation (40) with equation (41), we obtain: $\Delta p\frac{R}{2} \approx \frac{3}{2}\hbar$. Substituting this result into equation (32) yields

$$\Delta\lambda_{\mathrm{QC}} = \frac{3\hbar\lambda}{\mu_o cR}\left\{\left(1 - \frac{3C_1'}{\pi^2}\right) + \frac{sR^3\left(\frac{3C_2}{R} - \frac{1}{\alpha}\right)}{\pi^2\left(-sR + 2.0a_{\mathrm{B}(\infty)}\right)^2}\right\}. \tag{42}$$

The first term in the parenthesis (i.e., 1) represents the contribution of the exciton's kinetic energy (E_k) to the linewidth broadening. On the contrary, the second term (i.e.,$-\frac{3C_1'}{\pi^2}$) signifies the net contribution of the Coulomb interaction energy to the linewidth broadening. The third expression that contains $\left(\frac{3C_2}{R} - \frac{1}{\alpha}\right)$-term does describe the contribution of the e–h correlation energy to the linewidth broadening. It can be shown readily that the correlation effect (i.e., the 3rd term) is relatively negligible, in general. We will computationally show this point in section 3.1. Therefore, $\Delta\lambda_{\mathrm{QC}}$ is mainly contributed by the two opposing effects: (i) the linewidth broadening due to the repulsive kinetic energy of confined excitons and (ii) the linewidth narrowing caused by the net attractive Coulomb interaction. Then, we obtain

$$\Delta\lambda_{\mathrm{QC}} \approx \frac{3\hbar\lambda}{\mu_o cR}\left(1 - \frac{3C_1'}{\pi^2}\right) \equiv \Delta\lambda_{\mathrm{QC}}^{(\mathrm{KE})} - \Delta\lambda_{\mathrm{QC}}^{(\mathrm{Coul})}. \tag{43}$$

Equation (43) does explicitly state that the kinetic-energy term promotes the linewidth broadening while the Coulomb interaction tends to reduce the linewidth (i.e., linewidth narrowing). We will numerically examine the R-dependent linewidth and the three relative contributions in section 3.1.

3. Computational results and discussion

3.1. Two opposing contributions to linewidth broadening

As described in equation (42), the three distinct factors contribute to the linewidth broadening caused by the quantum confinement ($\Delta\lambda_{\mathrm{QC}}$). Before evaluating the three relative contributions to $\Delta\lambda_{\mathrm{QC}}$, one should find the effective Coulomb interaction coefficient (C_1'). PL emission measurement is typically carried out by dispersing MHP NPs in a low-permittivity (nonpolar) solvent having the relative dielectric permittivity of ε_r^s. In case of the prototypical emitter $MAPbBr_3$, the dispersing medium (solvent) is mainly composed of toluene ($\varepsilon_r^s \approx 2.5$) with a minor amount of surface-capping agent such as oleic acid [24]. According to the numerical calculations [21], the A_1 parameter appeared in equation (8) is -2.78 at $(\varepsilon_r^Q/\varepsilon_r^s) \approx 3$. Thus, the modified Coulomb interaction coefficient is: $C_1' = -\frac{1}{2}A_1 = +1.39$.

Let us evaluate the three relative contributions to $\Delta\lambda_{\mathrm{QC}}$ for a QD with its radius (R) equal to $a_{\mathrm{B}(\infty)}$ which is the exciton Bohr radius in the bulk unconfined state. In case of the $MAPbBr_3$ emitter, $a_{B(\infty)} \approx 5.0$ (nm) as described in section 2.2. In addition, $\alpha = -sR + 2.0a_{\mathrm{B}(\infty)} = -0.27R + 2.0a_{\mathrm{B}(\infty)} = 1.73a_{\mathrm{B}(\infty)}$, according to equation (30). Using this result, the 3rd term inside the grand parenthesis of equation (42) can be calculated as

$$\begin{aligned}&\frac{sR^3\left(\frac{3C_2}{R} - \frac{1}{\alpha}\right)}{\pi^2\left(-sR + 2.0a_{\mathrm{B}(\infty)}\right)^2}\\ &= \frac{0.27 \times \left(1.0a_{\mathrm{B}(\infty)}\right)^3\left\{\frac{3\times 0.498}{a_{\mathrm{B}(\infty)}} - \frac{1}{1.73a_{\mathrm{B}(\infty)}}\right\}}{9.87 \times \left(1.73a_{\mathrm{B}(\infty)}\right)^2}\\ &= 0.008.\end{aligned} \tag{44}$$

On the contrary, $1 : \frac{3C_1'}{\pi^2} = \frac{3\times 1.39}{9.87} = 1.0 : 0.42$, which is regardless of the QD size R. In other words, the 2nd line-narrowing Coulomb interaction term in equation (42) is ~42% of the 1st line-broadening term which is caused by the repulsive kinetic energy of a confined exciton. Thus, the relative contribution of the 3rd e–h correlation term, which is caused by the relative internal motion between an electron and a hole, is less than 1% and can be safely ignored in $\Delta\lambda_{\mathrm{QC}}$. Let us now evaluate the contribution of the 3rd correlation term for a QD at $R = 2a_{\mathrm{B}(\infty)}$ to see the effect of size increment on the linewidth broadening. In this case, $\alpha = -sR + 2.0a_{\mathrm{B}(\infty)} = -0.27R + 2.0a_{\mathrm{B}(\infty)} = -0.27 \times 2a_{\mathrm{B}(\infty)} + 2.0a_{\mathrm{B}(\infty)} = 1.46a_{\mathrm{B}(\infty)}$. Using this result, the 3rd term inside the grand parenthesis of equation (42) at $R = 2a_{\mathrm{B}(\infty)}$ can be computed as

$$\begin{aligned}&\frac{sR^3\left(\frac{3C_2}{R} - \frac{1}{\alpha}\right)}{\pi^2\left(-sR + 2.0a_{\mathrm{B}(\infty)}\right)^2}\\ &= \frac{0.27 \times \left(2.0a_{\mathrm{B}(\infty)}\right)^3\left\{\frac{3\times 0.498}{2a_{\mathrm{B}(\infty)}} - \frac{1}{1.46a_{\mathrm{B}(\infty)}}\right\}}{9.87 \times \left(1.46a_{\mathrm{B}(\infty)}\right)^2}\\ &= 0.006.\end{aligned} \tag{45}$$

The 3rd e–h correlation term is negligibly small and is even slightly reduced. According to our estimate, the 3rd e–h correlation term, regardless of the QD size, is too small to have any meaningful contribution to $\Delta\lambda_{\mathrm{QC}}$.

In view of the above computational results, $\Delta\lambda_{\mathrm{QC}}$ is mainly contributed by the two opposing effects: (i) the linewidth broadening due to the repulsive kinetic energy of confined excitons ($\Delta\lambda_{\mathrm{QC}}^{(\mathrm{KE})}$) and (ii) the linewidth narrowing caused by the attractive Coulomb interaction ($\Delta\lambda_{\mathrm{QC}}^{(\mathrm{Coul})}$). As briefly mentioned, the relative contribution remains at a constant value and can be quantitatively evaluated as

$$\frac{\Delta\lambda_{\mathrm{QC}}^{(\mathrm{Coul})}}{\Delta\lambda_{\mathrm{QC}}^{(\mathrm{KE})}} = \frac{3C_1'}{\pi^2} = \frac{3 \times 1.39}{9.87} = 0.42. \tag{46}$$

We have computed $\Delta\lambda_{\mathrm{QC}}$ for various values of R to assess the quantum-confinement effect on the net linewidth broadening of the protypical MHP emitter, $MAPbBr_3$. For this purpose, we

Table 1. The QD-size-dependent linewidth broadening of $MAPbBr_3$ due to the quantum confinement ($\Delta\lambda_{QC} \equiv \Gamma_{QC}$) with the two main contributions to $\Delta\lambda_{QC}$, namely, $\Delta\lambda_{QC}^{(KE)}$ and $\Delta\lambda_{QC}^{(Coul)}$. Herein, we adopted $\mu_o = 0.117m_o$ [23] in the calculation of $\Delta\lambda_{QC}^{(KE)}$, where m_o denotes the free-electron mass (9.11×10^{-31} kg). Notice that dimensionless (λ/R) values scale well with $\Delta\lambda_{QC}$ values over a wide range of R, which is theoretically supported by equation (43).

D(nm)	R(nm)	λ(nm)	$\Delta\lambda_{QC}^{(KE)}$ (nm)	$\Delta\lambda_{QC}^{(Coul)}$ (nm)	$\Delta\lambda_{QC}$(nm)
35	17.5	514	0.29	0.12	0.17
27	13.5	512	0.38	0.16	0.22
11	5.5	501	0.90	0.38	0.52
5	2.5	481	1.90	0.80	1.10
3	1.5	470	3.10	1.30	1.80

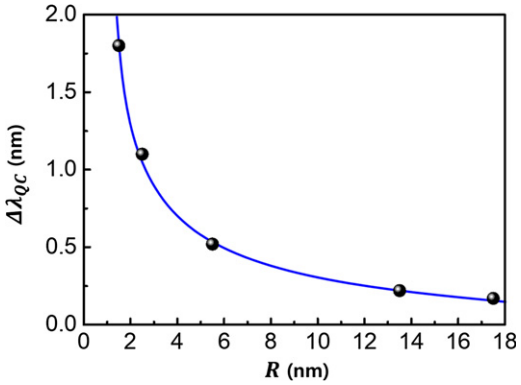

Figure 4. The net linewidth broadening due to the quantum confinement ($\Delta\lambda_{QC}$) plotted as a function of the QD size, R.

took the experimental values of the R-dependent PL emission wavelength (λ) as reported by Kim *et al* [24]. All of the calculated results, together with R-dependent λs, are summarized in table 1. As shown in figure 4, the net linewidth broadening due to the quantum confinement ($\Delta\lambda_{QC}$) increases rapidly beginning at the QD radius approximately equal to 6.5 nm which is $\sim 1.0\ a_{B(\infty)}$ ($a_{B(\infty)} \approx 5.0$ nm; section 2.2). However, $\Delta\lambda_{QC}$ is smaller than 2.0 nm even at the smallest synthesized QD of 1.5 nm (table 1). Indeed, $\Delta\lambda_{QC}$ of 2 nm is only 10% of the FWHM of 20 nm for ultrahigh color purity [5]. Thus, the linewidth broadening due to quantum confinement ($\Delta\lambda_{QC}$) is not a risk factor in the realization of MHP-based ultrahigh-quality next-generation LEDs.

3.2. Comparison with the exciton-LO phonon Fröhlich coupling

As described in section 1, the long-range Fröhlich coupling between exciton carriers and LO phonons is the predominant mechanism of linewidth broadening [9] with a vanishingly weak exciton-acoustic phonon coupling [25] in hybrid MHPs. In case of the $MAPbBr_3$ emitter, the net linewidth due to the carrier-LO phonon coupling [$\Gamma_{LO}(T)$] is 23.4 nm, including the background contribution from the temperature-independent inhomogeneous line broadening (Γ_o) of $\sim$4.5 nm at 300 K [9]. Thus, the linewidth due to the quantum confinement ($\Delta\lambda_{QC} = \Gamma_{QC}$) is much narrower than that of the Fröhlich coupling (Γ_{LO}). However, a significantly reduced long-range Fröhlich coupling with a concomitant linewidth narrowing is expected at a substantially reduced QD size. The effect of dimensional variation on the exciton-LO-phonon coupling and the consequent PL linewidth broadening has not been systematically investigated yet. Unlike localized excitons in GaAs/AlAs superlattices [26], a remarkably reduced long-range Fröhlich interaction was reported in the quasi-zero-dimensional ZnO QDs ($\sim$4 nm in the average size), as compared with the unconfined bulk ZnO crystals [27]. This reduced exciton-LO phonon coupling is accompanied with a linewidth narrowing (i.e., decrease in Γ_{LO}) at a fixed temperature since $\Gamma_{LO}(T) = \gamma_{LO}/\left\{e^{\hbar\omega_{LO}/k_BT} - 1\right\}$, where γ_{LO} is the exciton-LO phonon coupling strength. The reduced exciton-LO phonon coupling in a confined QD is closely related to a suppressed formation of the large Fröhlich polaron [6] which, in turn, is caused by inhibition in the development of a macroscopic electric-field in a QD smaller than a certain critical size. The formation of a macroscopic electric-field is necessary for an efficient exciton-LO phonon Fröhlich coupling [28, 29] which leads to a significant line broadening in MHPs [9]. Thus, search for a possible cross-over between Γ_{LO} and $\Gamma_{QC}(\equiv \Delta\lambda_{QC})$ at a substantially reduced QD size would be an interesting subject of future research.

4. Conclusions

We have theoretically shown that the PL linewidth broadening due to the quantum confinement ($\Delta\lambda_{QC}$) is mainly contributed by the two opposing effects: (i) the linewidth broadening due to the repulsive kinetic energy of confined excitons ($\Delta\lambda_{QC}^{(KE)}$) and (ii) the linewidth narrowing caused by the attractive Coulomb interaction ($\Delta\lambda_{QC}^{(Coul)}$). According to our prediction, the relative contribution essentially remains at a constant value and can be quantitatively evaluated as $\Delta\lambda_{QC}^{(Coul)}/\Delta\lambda_{QC}^{(KE)} = 0.42$, which is independent of the QD size (R) and the chemical nature of semiconductor emitter. On the contrary, the contribution of the quantum correlation term, which is caused by the internal relative motion between an electron and a hole in a given exciton, is estimated to be negligible. According to our theoretical prediction, the net linewidth broadening due to the quantum confinement ($\Delta\lambda_{QC}$) increases rapidly beginning at the QD radius approximately equal to 6.5 nm for the $MAPbBr_3$ emitter.

Acknowledgments

This research was supported by the National Research Foundation (NRF) grant funded by the Ministry of Science, ICT and Future Planning, Korea government (Grant Nos. NRF-2020R1A2C1013915 and NRF-2016R1A3B1908431).

Data availability statement

All data that support the findings of this study are included within the article (and any supplementary files).

ORCID iDs

Hyun Myung Jang https://orcid.org/0000-0002-1889-9515
Jinwoo Park https://orcid.org/0000-0002-8544-1643
Sungjin Kim https://orcid.org/0000-0001-7146-5479
Tae-Woo Lee https://orcid.org/0000-0002-6449-6725

References

[1] Kim Y-H, Cho H and Lee T-W 2016 *Proc. Natl Acad. Sci. USA* **113** 11694
[2] Tan Z-K *et al* 2014 *Nat. Nanotechnol.* **9** 687
[3] Kim Y-H, Cho H, Heo J H, Kim T-S, Myoung N, Lee C-L, Im S H and Lee T-W 2015 *Adv. Mater.* **27** 1248
[4] Cho H *et al* 2015 *Science* **350** 1222
[5] Kim Y H, Kim J S and Lee T W 2018 *Adv. Mater.* **31** 1804595
[6] Jang H M, Kim J-S, Heo J-M and Lee T-W 2020 *APL Mater.* **8** 020904
[7] Rudin S, Reinecke T L and Segall B 1990 *Phys. Rev.* B **42** 11218
[8] Lee J, Koteles E S and Vassell M O 1986 *Phys. Rev.* B **33** 5512
[9] Wright A D, Verdi C, Milot R L, Eperon G E, Pérez-Osorio M A, Snaith H J, Giustino F, Johnston M B and Herz L M 2016 *Nat. Commun.* **7** 11755
[10] Park M-H *et al* 2017 *Nano Energy* **42** 157
[11] Zhang F, Zhong H, Chen C, Wu X-g, Hu X, Huang H, Han J, Zou B and Dong Y 2015 *ACS Nano* **9** 4533
[12] Zheng K *et al* 2015 *J. Phys. Chem. Lett.* **6** 2969
[13] Schmidt L C, Pertegás A, González-Carrero S, Malinkiewicz O, Agouram S, Mínguez Espallargas G, Bolink H J, Galian R E and Pérez-Prieto J 2014 *J. Am. Chem. Soc.* **136** 850
[14] Kim Y, Yassitepe E, Voznyy O, Comin R, Walters G, Gong X, Kanjanaboos P, Nogueira A F and Sargent E H 2015 *ACS Appl. Mater. Interfaces* **7** 25007
[15] Jang D M, Park K, Kim D H, Park J, Shojaei F, Kang H S, Ahn J-P, Lee J W and Song J K 2015 *Nano Lett.* **15** 5191
[16] Anikeeva P O, Halpert J E, Bawendi M G and Bulović V 2009 *Nano Lett.* **9** 2532
[17] Kayanuma Y 1986 *Solid State Commun.* **59** 405
[18] Kayanuma Y 1988 *Phys. Rev.* B **38** 9797
[19] Einevoll G T 1992 *Phys. Rev.* B **45** 3410
[20] Brus L E 1984 *J. Chem. Phys.* **80** 4403
[21] Takagahara T 1993 *Phys. Rev.* B **47** 4569
[22] Romestain R and Fishman G 1994 *Phys. Rev.* B **49** 1774
[23] Galkowski K *et al* 2016 *Energy Environ. Sci.* **9** 962
[24] Kim Y-H *et al* 2017 *ACS Nano* **11** 6586
[25] Fu M, Tamarat P, Trebbia J-B, Bodnarchuk M I, Kovalenko M V, Even J and Lounis B 2018 *Nat. Commun.* **9** 3318
[26] Zhao H, Wachter S and Kalt H 2002 *Phys. Rev.* B **66** 085337
[27] Ning J Q, Zheng C C, Zhang X H and Xu S J 2015 *Nanoscale* **7** 17482
[28] Zhu X-Y and Podzorov V 2015 *J. Phys. Chem. Lett.* **6** 4758
[29] Peeters F M and Devreese J T 1985 *Phys. Rev.* B **31** 4890